Supporting information: On the Redox Mechanism of Methanol Carbonylation on the Dispersed ReO_x/SiO_2 Catalyst

Neil D. Tran and Alexander V. Mironenko*
Department of Chemical and Biomolecular Engineering, University of Illinois Urbana-Champaign, Urbana, Illinois 61801, United States
*Email: alexmir@illinois.edu

Section S1. Generation and validation of catalytic site models

A catalytic site model consisting of -$OReO_3$ anchored to the SiO_2 support was carved from the amorphous silica model reported previously.[1] The amorphous silica slab contains more than 10,000 atoms and thus is not feasible to study using DFT calculations. Therefore, the following algorithm was used to generate the truncated structures:

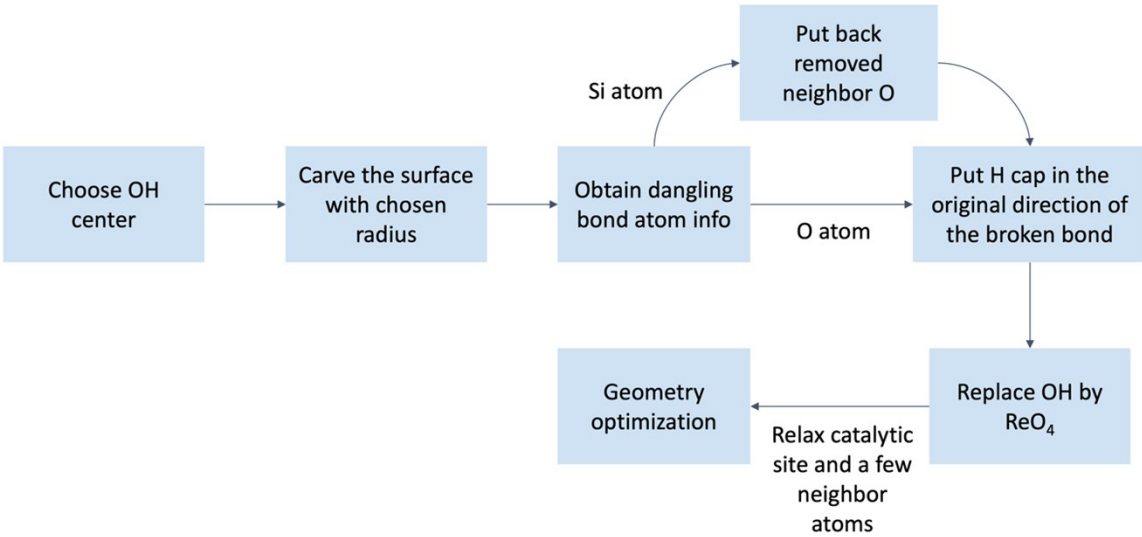

Scheme S1. Algorithm for generating cluster models of a catalytic site.

The carving radius was chosen based on the convergence of the grafting energy of ReO_4 on the surface:

$$E_{graft} = (E_{Si-O-ReO_3} + E_{H_2O}) - (E_{Si-OH} + E_{HReO_4})$$

In cluster comparison calculations, spin-polarized periodic DFT was employed using VASP 6.2.0[2, 3] at the PBE[4] level of theory using D3[5] dispersion correction with Becke-Johnson damping[6]. The projector-augmented wave[7, 8] method was employed to describe core-valence electron interactions. A 400 eV plane wave energy cutoff and a Γ-point were employed for both small and large cluster models. A 25 Å x 25 Å x 25 Å unit cell was used to prevent interactions between two nearest images. A Gaussian smearing with 0.03 eV width was used. Convergence criteria were set to 10^{-5} eV for the self-consistent field (SCF) loop and 0.02 eV/Å for the ionic relaxation loop. VASP results for the large model were also compared to calculations of the small model using ORCA software[9] at the PBE/ma-def2-TZVP[10] level. Transition state optimization in VASP was performed by the improved dimer method[11] implemented in VASP, with the force and SCF iteration break conditions of 0.02 eV/Å and 10^{-7} eV, respectively.

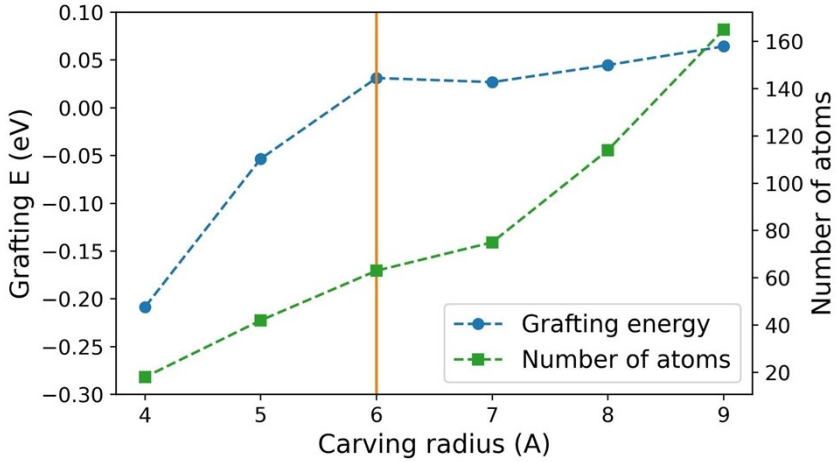

Figure S1. Convergence checks of carving radius. The carving radius is 6 Å was chosen as it nearly reaches the convergence and minimizes the number of atoms in the structure to reduce the computational cost.

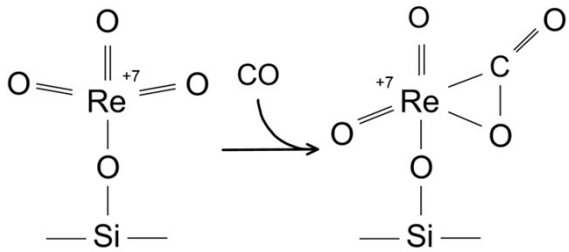

Figure S2. CO binding reaction used for validating reactivity of the small cluster model.

Table S1. Geometric properties of small and large catalytic site models.

	Large model	Small model		Experiment[2]
Method / Bond	VASP PBE/400 eV cutoff	VASP PBE/400 eV cutoff	ORCA PBE/ma-def2-TZVP	EXAFS
Re=O (Å)	1.73	1.73	1.72	1.69
Re-O (Å)	1.89	1.87	1.87	1.77

Table S2. Electronic energy barrier and reaction energy of CO binding on small and large clusters.

	Large model (PBE)	Small model (PBE)	
Method	VASP PBE/400 eV cutoff	VASP PBE/400 eV cutoff	ORCA PBE/ma-def2-TZVP
Activation barrier (eV)	0.96*	0.91	0.96
Reaction energy (eV)	-0.13	-0.19	-0.01

*The difference with the 2.3 eV barrier reported in Figure 1 of the main text is mainly due to the neglect of entropic and temperature effects (~ 1 eV) and partially due to barrier underestimation at the PBE level of DFT theory in comparison with the hybrid theory (~ 0.3 eV).

Table S3. Geometric properties of the catalytic site grafted onto both the simple -$Si(OH)_3$ model and larger supports featuring a randomly selected silanol group on the amorphous silica surface. The larger cluster was truncated at the third-nearest oxygen atom to the Re center and capped with H atoms. Geometry optimizations were performed using the PBE/ma-def2-TZVP basis set to enable direct comparison with the simplified cluster geometry. The electronic activation barriers of C-C coupling on the complex $Re(=O)(CO)(CH_3)(OH)$ were calculated using ωB97x-D3BJ/ma-def2-TZVP for direct comparison with the value obtained for the simplified model as mentioned in the main text. Red = O, white = H, yellow = Si, grey = C, and blue = Re.

		Geometry (PBE/ma-def2-TZVP)		**Barrier (eV)** (ωB97x-D3BJ / ma-def2-TZVP)
		Re=O (Å)	**Re-O (Å)**	
Simple cluster		1.72	1.87	1.364
Three-nearest neighbor cluster	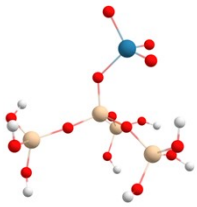	1.72	1.87	1.435
		1.72	1.85	1.373
	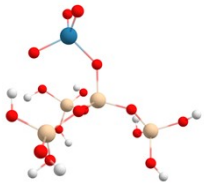	1.72	1.86	1.316

Section S2. Estimation of the energetic span from experimental kinetic data

For a reaction that is first order in methanol and CO, the expression for the turnover frequency (TOF) is

$TOF = k_{eff} x_{CO} x_{MeOH}$,

where k_{eff} is the effective rate constant, which can be defined as

$$k_{eff} = \frac{k_B T}{h} e^{-\frac{\delta E}{RT}},$$

where δE is the energetic span of the catalytic cycle, T is the temperature of the reaction, k_B is the Boltzmann's constant, h is the Planck's constant, R is the ideal gas constant, and x_i is a molar fraction of species i.

From the kinetic data obtained by Qi and coworkers[12], the TOF of the 1% Re/SiO_2 at 280°C is approximately $7.08 \cdot 10^{-3}$ s^{-1} (rate = 0.038 mmol s^{-1} g_{Re}^{-1}) with 30 mbar of CO and 30 mbar of CH_3OH (corresponding molar fractions of 0.03). Consequently, $k_{eff} = 7.87\ s^{-1}$. Therefore, the energetic span estimated from the experimental measured rate is

$$\delta E = -RT \ln\left(\frac{k_{eff}\, h}{kT}\right) = -8.63 \times 10^{-5} \times (553.15) \times \ln\left(\frac{7.87 \times 6.626 \times 10^{-34}}{1.38 \times 10^{-23} \times 553.15}\right) \approx 1.34\ eV$$

Section S3. Model mechanisms involving the Re^{+7} catalytic site

Section S3.1: Proposed mechanism by Qi et al.

Qi and colleagues proposed a mechanism based on experimental evidence showing that Re maintains the +7 oxidation state under reaction conditions.[13] Consequently, our initial approach involved conducting DFT calculations to pinpoint the proposed intermediate. Despite numerous attempts, we were unable to locate the intermediate shown on the left in Figure S3a, as CO does not bind to Re-CH_3. Upon inspecting the LUMO of the methoxy species (the intermediate on the right), we observed no symmetry compatibility with the HOMO of the CO molecule, and the HOMO-LUMO gap is notably large. This leads us to conclude that there is no overlap between CO and CH_3, indicating that CO cannot bind to the CH_3 end of the methoxy group. Perhaps this is not very surprising, since the middle C atom cannot be 5-valent. Therefore, we discarded this hypothesis and explored other possibilities.

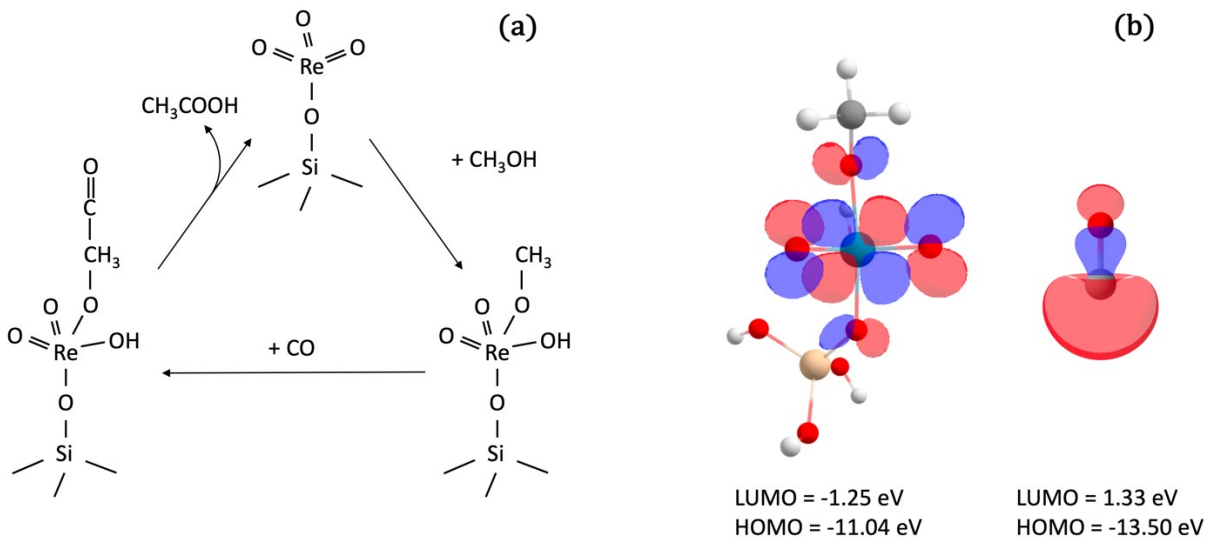

Figure S3. (a) Proposed mechanism by Qi et al., 2020, (b) HOMO of intermediate on the right and LUMO of CO molecule (iso-surface value = 0.08). The HOMO is localized on Re and neighboring O, which indicates no interaction between CO and C-end of -OCH_3 group. Red = O, White = H, Yellow = Si, Grey = C, and Blue = Re.

Section S3.2: Proposed mechanism involving the formation of ketene species

We hypothesized the mechanism involving the formation of ketene species (-CH_2CO) as an intermediate after the C-C coupling step, as reported in a DFT study on the dimethyl ether carbonylation over HPA (Scheme S2). However, Figure S4 shows that the Gibbs free energy of the intermediate corresponding to the ketene species is 1.99 eV, which makes this mechanism infeasible at the experimental reaction conditions. Therefore, we also reject this hypothesis.

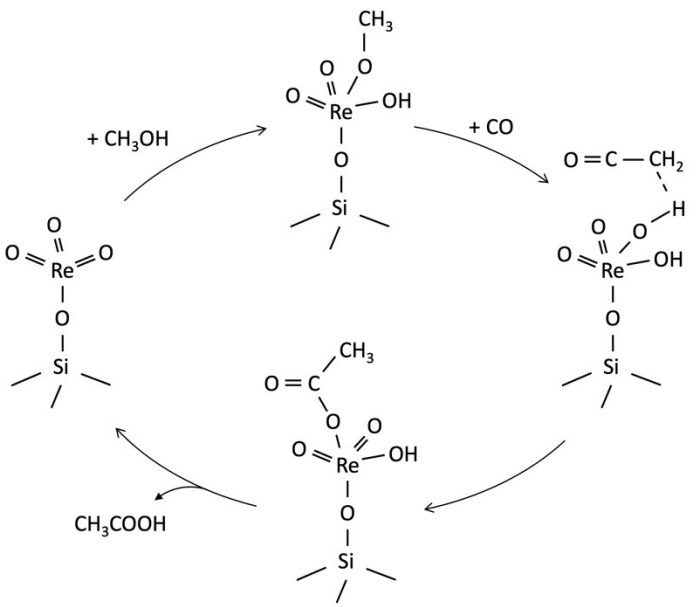

Scheme S2. The proposed mechanism involving ketene species inspired by the study of Cai et al[14].

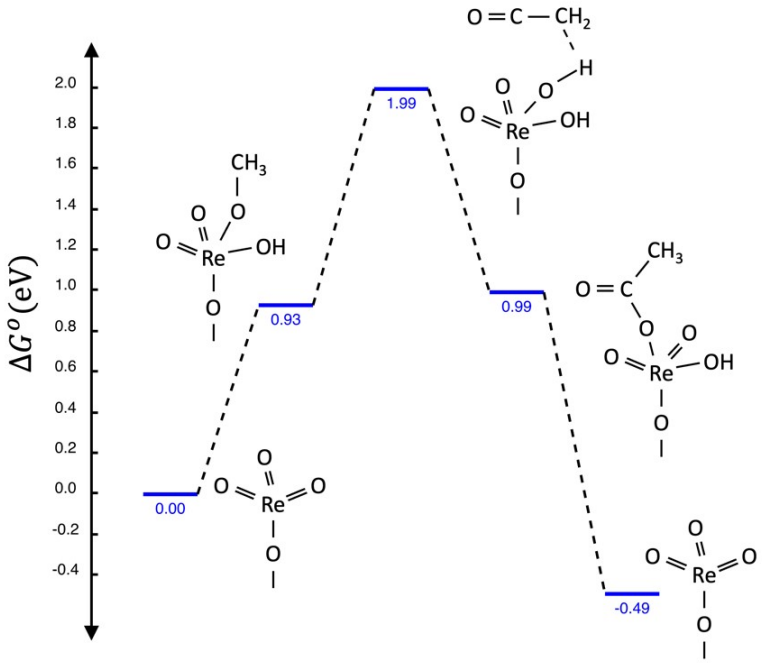

Figure S4. Gibbs free energy profile of the pathway associated with ketene species. No transition states were computed since the mechanism can be ruled out from thermodynamics alone.

Section S4. The meta-stable -OCO species

As the -OCO bidentate species was observed during our investigation of the Re(VII) reduction, we proposed a mechanism involving this species which forms the C-C bond with -CH_3 group (Scheme S3). Although we were able to optimize the intermediate Re(O)(CH_3)(OH)(=OCO), it was found to dissociate easily to form CO_2 with no barrier (Figure S5). Moreover, the TS structure for the C-C coupling step could not have been located that would satisfy the criterion of having a single imaginary mode associated with bond formation.

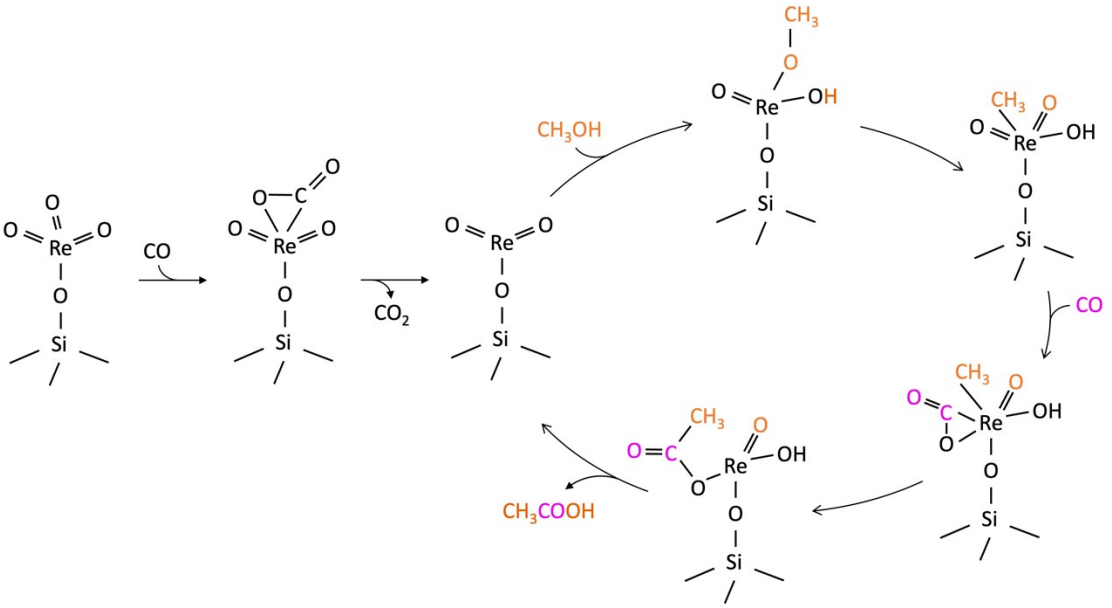

Scheme S3. The hypothetical -OCO pathway. The pathway involves an induction process of reducing Re^{+7} to Re^{+5}. The bidentate -OCO intermediate is meta-stable.

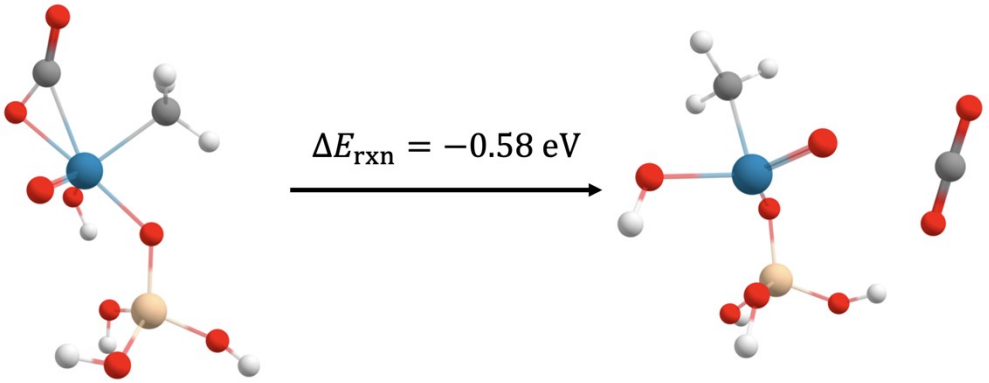

Figure S5. The dissociation of the -OCO ligand to form CO_2 is barrierless. The transition metal complex is reduced to a +3 oxidation state. The electronic energy of the reaction is -0.58 eV, indicating that the state involving the (-OCO) ligand is meta-stable.

Section S5. The Eley-Rideal mechanism for C-C coupling.

We propose the direct C-C coupling of gas-phase CO with the -CH_3 group bound to Re center (Scheme S4). The barrier for the Eley-Rideal C-C coupling step is very high (2.55 eV), ruling out the mechanism in favor of the co-bound -CH_3 and -CO to the Re center.

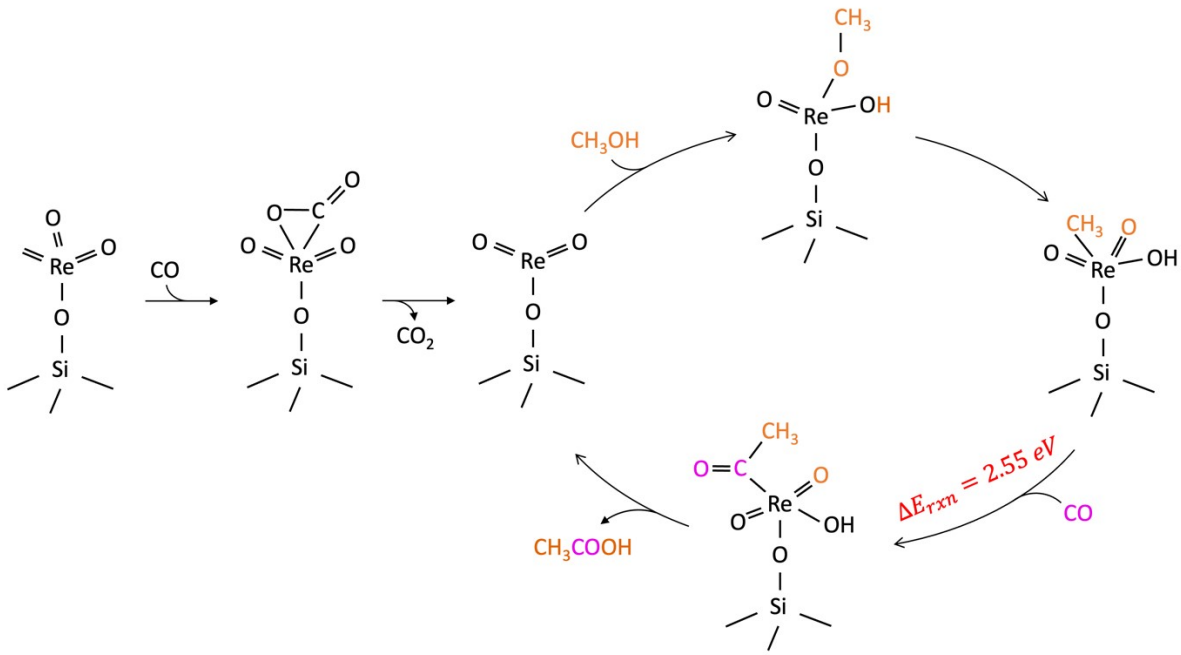

Scheme S4. The Eley-Rideal mechanism for the direct C-C coupling between gas-phase CO and the -CH_3 group. The electronic barrier of the C-C coupling step is 2.55 eV, suggesting that the mechanism is unfeasible.

Section S6. NBO analysis of proposed elementary steps

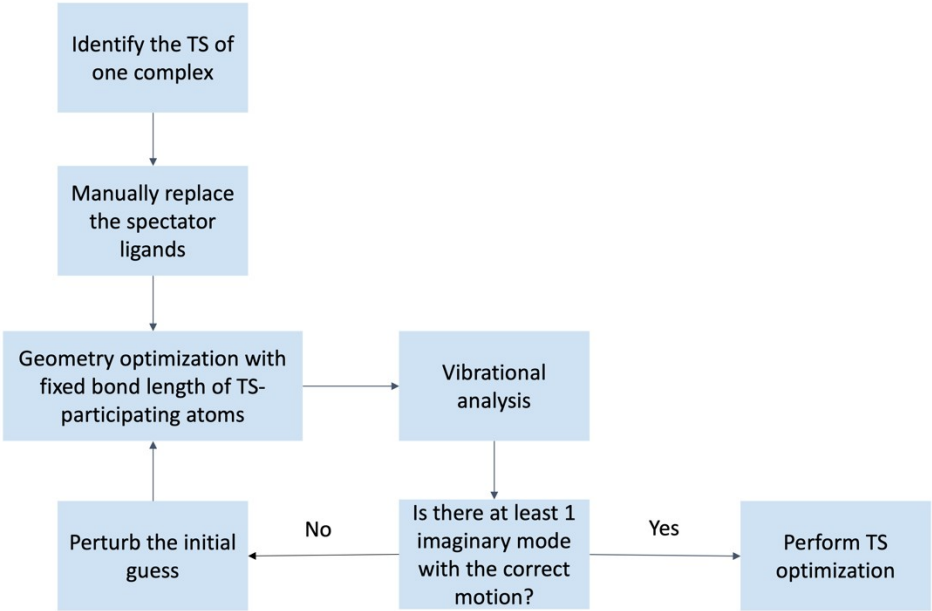

Scheme S5. Algorithm of ligand screening for each proposed elementary step.

Table S4. Rhenium-center's lone pair (LP) occupancy and the most significant donor-acceptor interaction represented by the largest second-order perturbative energy (E(2)) in high and low oxidation-state TS complexes of the C-C coupling step. Maximum occupancy is 2 for the ideal Lewis bonding pattern. Low occupancy indicates delocalization of the electron pair into an acceptor NBO.

Complex	LP	Occupancy	E(2) (kcal/mol)	Acceptor
Re(=O)(CO)(CH_3)(OH)	1	1.95183	107.35	BD*(1) Re≡O
Re(=O)(CO)(CH3)(OCH_3)	1	1.94858	151.57	BD*(1) Re≡O
Re(=O)(CO)(CH_3)(CH_3)	1	1.92983	79.51	BD*(1) Re≡O
Re(=O)(CO)(CH_3)($COCH_3$)	1	1.71085	27.37	BD*(2) O-C
Re(=O)(CO)(CH_3)($OCOCH_3$)	1	1.95867	60.77	BD*(1) Re-O
Re(CO)(CO)(CH_3)(OH)	1 2	1.53079 1.12927	101.40 902.22	BD*(1) O-C BD*(1)Re-C*
Re(CO)(CO)(CH_3)(OCH_3)	1 2	1.50139 1.07448	98.54 1827.67	BD*(1) O-C BD*(1)Re-C*

$Re(CO)(CO)(CH_3)(CH_3)$	1	1.56613	76.57	BD*(1) O-C
	2	0.93380	2149.55	BD*(1)Re-C*
$Re(CO)(CO)(CH_3)(COCH_3)$	1	1.55975	69.56	BD*(1) O-C
	2	0.93721	3614.33	BD*(1)Re-C*
$Re(CO)(CO)(CH_3)(OCOCH_3)$	1	1.73482	40.89	BD*(2) O-C*
	2	1.72398	64.99	BD*(2) O-C

**Carbon with the asterisk is the carbon participating in the C-C coupling process. BD* means antibonding orbital.*

Table S5. Electronic O-H scission energy in adsorbed methanol for various ligand configurations.

Reaction	**Electronic reaction energy (eV)**
$Re(=O)_2(CH_3OH) \rightarrow Re(=O)(OH)(OCH_3)$	-0.262
$Re(=O)(CH_3OH) \rightarrow Re(OH)(OCH_3)$	-0.729
$Re(=O)(CH_3OH)(CO) \rightarrow Re(OH)(OCH_3)(CO)$	-1.262

Table S6. Re-center's lone pair (LP) occupancy and the most significant donor-acceptor interaction represented by the largest second-order perturbative energy (E(2)) in high and low oxidation-state complexes (with and without CO) for C-O bond cleavage step. Maximum occupancy is 2 for the ideal Lewis's bonding pattern. Low occupancy indicates the delocalization of the electron pair to the acceptor NBO.

Complex	**LP**	**Occupancy**	**E(2) (kcal/mol)**	**Acceptor**
$Re(=O)(OCH_3)(OH)$	1	1.60013	170.88	BD*(1) C-O*
$Re(=O)(OCH3)(OCH_3)$	1	1.21011	622.43	BD*(1) C-O*
$Re(=O)(OCH_3)(CH_3)$	1	1.66797	89.15	BD*(1) C-O*
$Re(=O)(OCH_3)(COCH_3)$	1	1.62606	128.38	BD*(1) C-O*
$Re(=O)(OCH_3)(OCOCH_3)$	1	1.72951	69.86	BD*(1) O-C
$Re(CO)(OCH_3)(OH)$	1	1.51943	116.42	BD*(1) Re-C
$Re(CO)(OCH_3)(OCH_3)$	1	1.72016	72.19	BD*(1) O-C

Re(CO)(OCH_3)(CH_3)	1	1.45525	78.56	BD*(1) Re-C
Re(CO)(OCH_3)($COCH_3$)	1	1.65750	41.65	BD*(1) O-C
Re(CO)(OCH_3)($OCOCH_3$)	1	1.73937	54.12	BD*(1) O-C

**C-O* indicates the antibonding of atoms participating in the TSs. BD* means antibonding orbital.*

Table S7. Relative electronic energies of reactants, TS, and products for C–O bond scission in singlet and triplet states for Y = vacant.

Reactant complex	Spin states	Reactant	TS	Product
Re(OCH_3)(OCH_3)	Singlet	0.446	1.680	-1.562
	Triplet	0	1.444	-1.393
Re(OCH_3)(OH)	Singlet	0.523	1.492	-1.602
	Triplet	0	1.442	-1.229
Re(OCH_3)(CH_3)	Singlet	0.290	1.274	-1.899
	Triplet	0	1.474	-1.506
Re(OCH_3)($COCH_3$)	Singlet	0	1.037	-2.140
	Triplet	0.079	1.980	-1.200
Re(OCH_3)($OCOCH_3$)	Singlet	0.352	1.636	-1.655
	Triplet	0	1.426	-1.343

**The reference state is the most stable spin state of the reactant. Energy is in eV.*

Table S8. Gibbs free energy of CO binding to Re(OCH_3)(X) complexes

Complex	$\Delta G^{o}_{CO\ binding}$ **(eV)**
-Re(OCH_3)(OH)	-1.179
-Re(OCH_3)(OCH_3)	-1.239
-Re(OCH_3)(CH_3)	-1.341
-Re(OCH_3)($COCH_3$)	-1.367
-Re(OCH_3)($OCOCH_3$)	-1.089

Table S9. NBO analysis of C–O bond scission transition state complexes with Y = vacant. For open-shell calculations (triplet TSs), NBO was performed separately for alpha and beta spin orbitals (occupancy from 0 to 1). For closed-shell calculations (singlet TSs), electrons are paired (occupancy from 0 to 2), and a single set of natural orbitals is generated for the entire system. This table lists low-occupancy lone electrons associated with the atoms involved in the transition state (i.e., Re, O, and C, where O and C belong to the reacting $–OCH_3$ ligand of the complex).

Complex	Atom	Spin	Occupancy	E(2) (kcal/mol)	Acceptor	Note
$Re(OCH_3)(OH)$ (triplet)	Re	α	0.70694	910.19	BD* Re – O	Reactive O
	O	β	0.86742	64.04	LV Re	
		β	0.63070	86.55	BD* Re – C	
$Re(OCH_3)(OCH_3)$ (triplet)	Re	α	0.62592	979.19	BD* Re – O	O of spectator OCH_3
	O	β	0.86875	13.73	BD* Re – O	O of spectator OCH_3
		β	0.63018	85.68	BD* Re – C	Reactive C
$Re(OCH_3)(OCOCH_3)$ (triplet)	O	α	0.70208	85.08	BD* Re – C	
		β	0.61089	95.08	BD* Re – C	

Complex	LP	Occupancy	E(2) (kcal/mol)	Acceptor
$Re(OCH_3)(CH_3)$ (singlet)	1	1.96821	19.14	BD*(1) Re- C
$Re(OCH_3)(COCH_3)$ (singlet)	1 2	1.80022 1.69056	63.99 42.12	BD*(1) Re-C BD*(1) Re-O

** LP = Lone Pair, BD = Bonding, BD* = Anti-bonding, LV = Lone valency (unfilled non-bonding)*

Table S10. Ligand screening results of the C-O bond formation to form the ($-OCOCH_3$) ligand for plotting the histogram in Figure 6a.

Reactant complex	$\Delta E^{\ddagger}$ (eV)	ΔE_{rxn} (eV)
$ReO-COCH_3-OH$	1.27	1.33
$ReO-COCH_3-OH-Met$	2.44	1.13
$ReO-COCH_3-OH-H2O$	1.66	1.15
$ReO-COCH_3-OH-CO$	1.96	1.24
$ReO-COCH_3-OH-CO-CO$	1.71	-1.47
$ReO-COCH_3-OH-CO-Met$	1.50	-1.10
$ReO-COCH_3-OH-OCH_3-OH$	0.71	-1.22
$ReO-COCH_3-OH-CH_3-OH$	0.56	-0.76
$ReO-COCH_3-OCH_3$	2.33	1.65
$ReO-COCH_3-OCH_3-CO$	1.95	1.03
$ReO-COCH_3-OCH_3-CO-H2O$	1.70	-1.00
$ReO-COCH_3-OCH_3-CO-CO$	1.47	-1.84
$ReO-COCH_3-OCH_3-Met$	2.29	1.20
$ReO-COCH_3-OCH_3-CO-Met$	2.10	-1.00
$ReO-COCH_3-OCH_3-H2O$	1.74	1.19

ReO-$COCH_3$-CH_3-CO	2.21	-0.23
ReO-$COCH_3$-CH_3-Met	2.51	1.73
ReO-$COCH_3$-CH_3-CO-CO	1.70	-1.62
ReO-$COCH_3$-$COCH_3$	2.31	1.04
ReO-$COCH_3$-$COCH_3$-CO	1.86	-0.90
ReO-$COCH_3$-$COCH_3$-Met	2.24	1.25
ReO-$COCH_3$-$COCH_3$-H2O	2.28	1.58
ReO-$COCH_3$-$COCH_3$-CO-Met	1.77	-1.10
ReO_2-$COCH_3$-CH_3	0.27	-1.60

Table S11. Ligand screening results of the C-O bond formation to directly form AA for plotting the histogram in Figure 6a.

Reactant complex	$\Delta E^{\ddagger}$ **(eV)**	ΔE_{rxn} **(eV)**
ReO-$COCH_3$-OH	1.19	1.02
ReO-$COCH_3$-OH-CO-CO	1.78	0.16
ReO-$COCH_3$-OH-CO-Met	1.89	0.97
Re-$COCH_3$-OH-OCH_3-OH	1.03	0.96
Re-$COCH_3$-OH-OH-OH	1.15	0.89
Re-$COCH_3$-OH-CH_3-OH	1.00	0.95
Re-$COCH_3$-OH-CH_3-CH_3	1.45	0.48
Re-$COCH_3$-OH-OCH_3-$COCH_3$	0.93	0.86
Re-$COCH_3$-OH-OCH_3-CH_3	0.92	0.07
Re-$COCH_3$-OH-OCH_3-OCH_3	1.02	0.14
Re-$COCH_3$-OH-$COCH_3$-OH	0.75	0.67
Re-$COCH_3$-OH-$COCH_3$-$COCH_3$	0.17	-0.15
Re-$COCH_3$-OH-CO-CO	0.77	0.30

Table S12. Rhenium center's lone pair (LP) occupancy and the most significant donor-acceptor interaction represented by the largest second-order perturbative energy (E(2)) of different TS complexes for the C-O bond formation step.

Complex	LP	Occupancy	E(2) (kcal/mol)	Acceptor
$Re(OH)(COCH_3)(OH)(OH)$	1	1.97439	104.23	BD*(1) Re-O
$Re(OH)(COCH_3)(OCH_3)(OCH_3)$	1	1.95000	27.12	BD*(1) Re-O
$Re(OH)(COCH_3)(CH_3)(CH_3)$	1	1.94594	38.02	BD*(1) Re-C
$Re(OH)(COCH_3)(COCH_3)(COCH_3)$	1	1.70742	31.65	BD*(2) O-C
$Re(OH)(COCH_3)(CO)(CO)$	1	1.64435	41.44	BD*(1) O-C
	2	1.53135	54.34	BD*(3) O-C

**BD* means antibonding orbital.*

Table S13. The occupancy of natural bonding orbitals between metal and the reactive ligands in the AA formation step ($-COCH_3$ and -OH). Maximum occupancy is 2. Low occupancy indicates weak bonding.

Complex	Re-$COCH_3$ BD	Re-OH BD
$Re(OH)(COCH_3)(OH)(OH)$	1.95656	1.97690
$Re(OH)(COCH_3)(OCH_3)(OCH_3)$	1.95639	1.98074
$Re(OH)(COCH_3)(CH_3)(CH_3)$	1.94702	1.97668
$Re(OH)(COCH_3)(COCH_3)(COCH_3)$	1.91155	1.97483
$Re(OH)(COCH_3)(CO)(CO)$	1.86520	1.93447

Section S7. Constructing reaction pathways based on ligand screening data

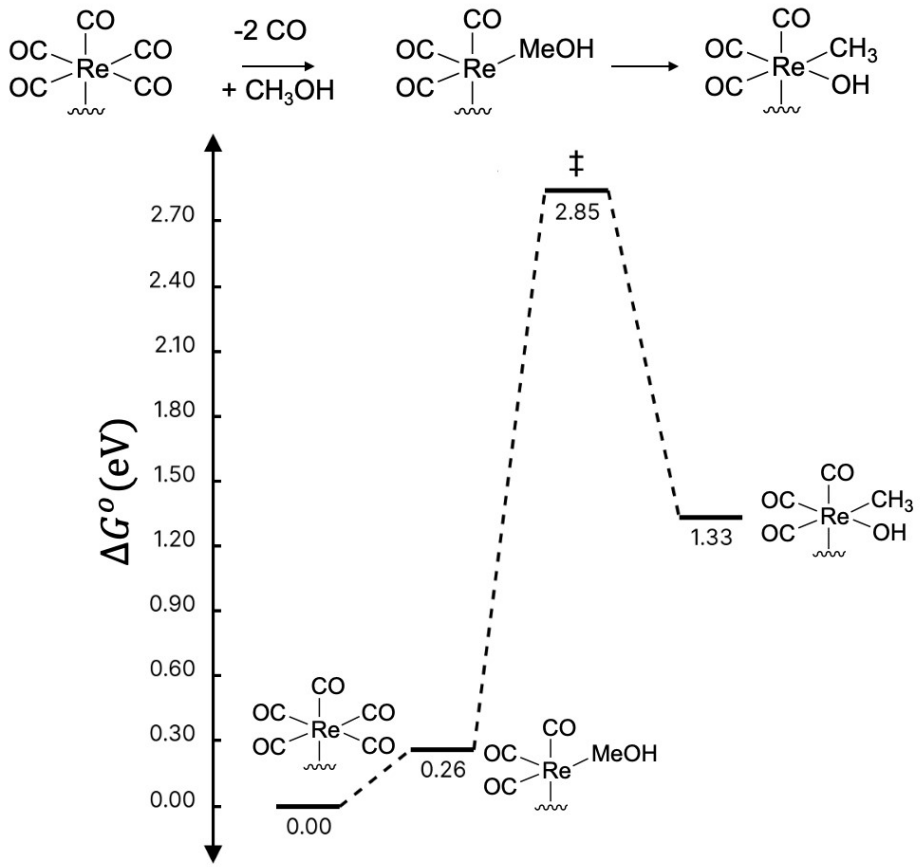

Figure S6. C-O bond scission on the Re (I) center. Direct C-O bond scission of methanol is associated with the extremely high barrier (2.85 eV), indicating the infeasibility of this pathway. This result is consistent with the prediction in Section 3c of the main text.

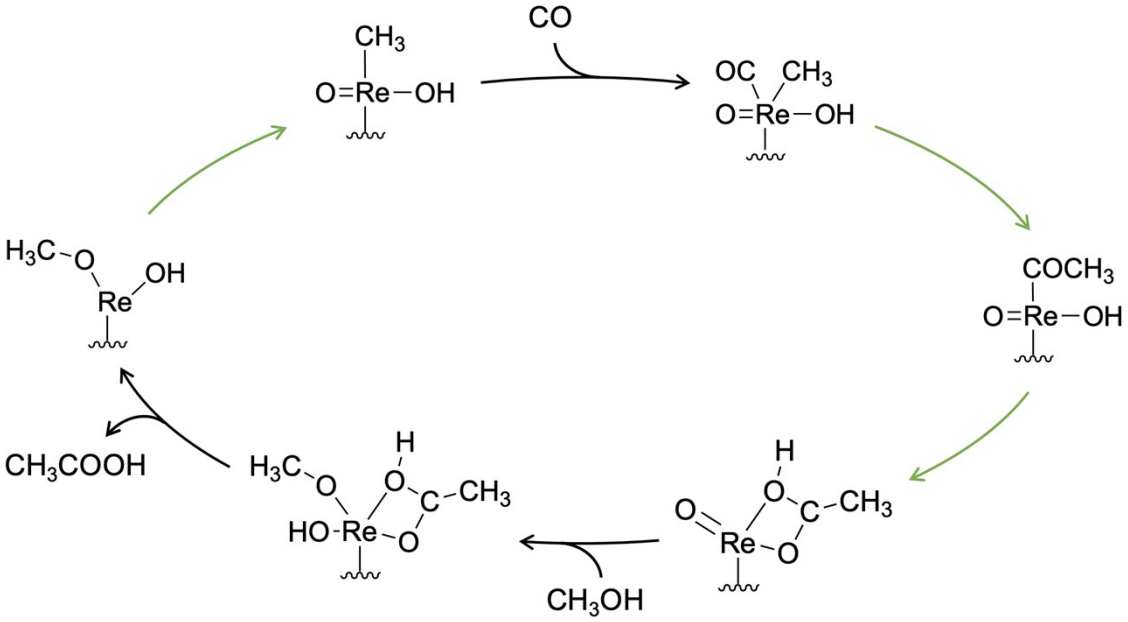

Scheme S6. Catalytic cycle involving the Re(=O)(CO)(CH_3)(OH) intermediate.

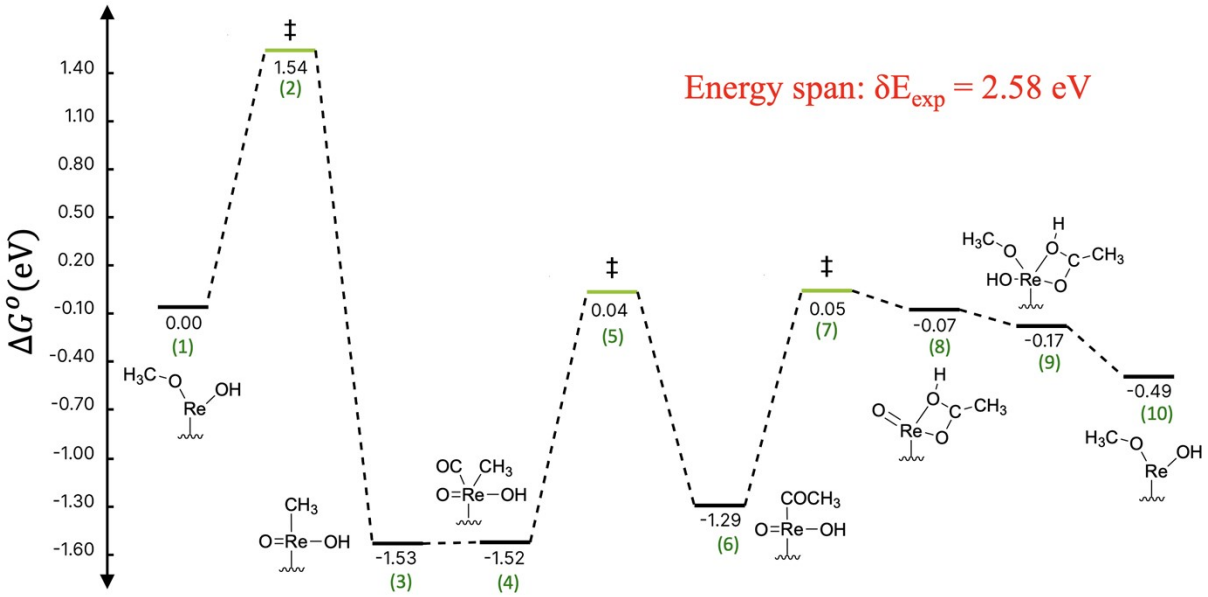

Figure S7. Gibbs free energy profile of the reaction cycle as presented in **Scheme S6**. States (1)/(10), (2), and (9) are depicted in their triplet spin states due to their more favorable energetics. A fast spin-crossing rate is assumed for transitions between spin states.[15, 16]

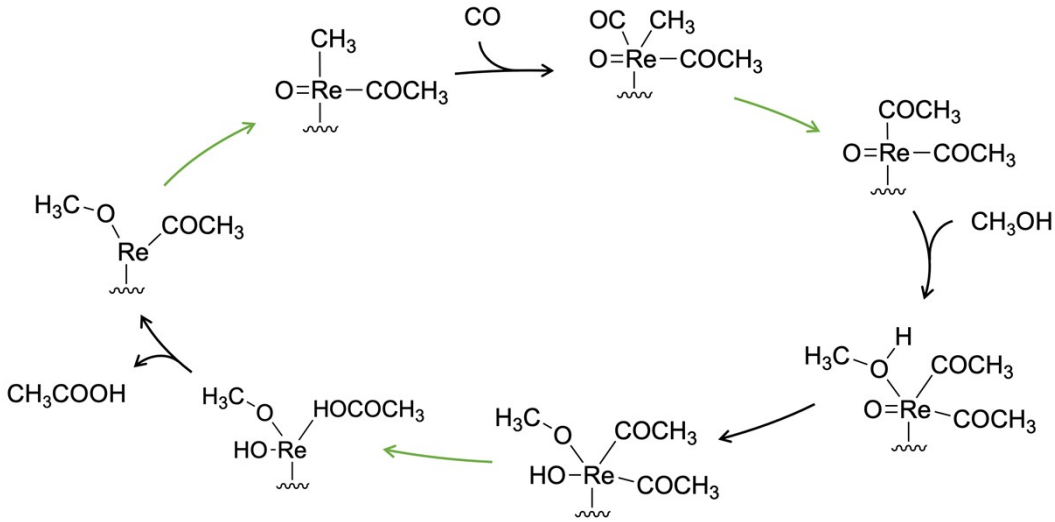

Scheme S7. Reaction cycle starting from $Re(OCH_3)(COCH_3)$. This intermediate was chosen due to the lowest C-O scission reaction barrier.

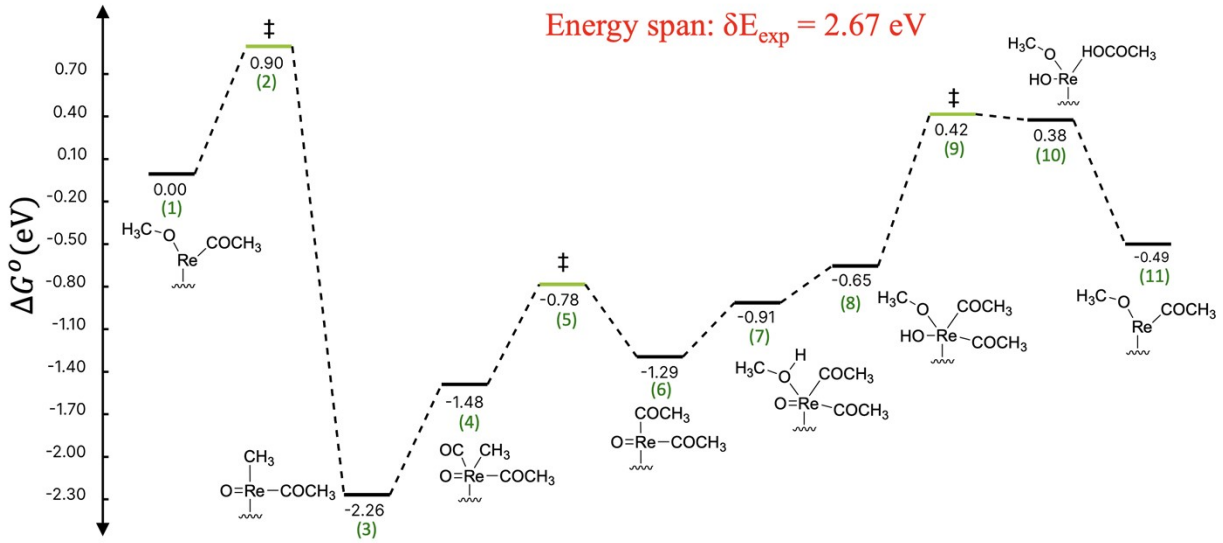

Figure S8. Gibbs free energy profile of the reaction cycle as presented in **Scheme S7**. All states are singlet; no spin-forbidden reactions are assumed to occur.

References:

(1) Garofalini, S. H. Molecular dynamics computer simulations of silica surface structure and adsorption of water molecules. *Journal of Non-Crystalline Solids* **1990**, *120* (1), 1-12. DOI: 10.1016/0022-3093(90)90184-N (acccessed 2022/02/16/18:10:57). From ScienceDirect.

(2) Kresse, G.; Furthmüller, J. Efficient iterative schemes for ab initio total-energy calculations using a plane-wave basis set. *Physical Review B* **1996**, *54* (16), 11169-11186. DOI: 10.1103/PhysRevB.54.11169 (acccessed 2022/04/10/16:51:23). From DOI.org (Crossref).

(3) Kresse, G.; Furthmüller, J. Efficiency of ab-initio total energy calculations for metals and semiconductors using a plane-wave basis set. *Computational Materials Science* **1996**, *6* (1), 15-50. DOI: 10.1016/0927-0256(96)00008-0 (acccessed 2022/04/10/16:50:41). From DOI.org (Crossref).

(4) Perdew, J. P.; Burke, K.; Ernzerhof, M. Generalized Gradient Approximation Made Simple. *Physical Review Letters* **1996**, *77* (18), 3865-3868. DOI: 10.1103/PhysRevLett.77.3865 (acccessed 2024/03/30/21:59:24). From DOI.org (Crossref).

(5) Grimme, S.; Antony, J.; Ehrlich, S.; Krieg, H. A consistent and accurate ab initio parametrization of density functional dispersion correction (DFT-D) for the 94 elements H-Pu. *The Journal of Chemical Physics* **2010**, *132* (15), 154104. DOI: 10.1063/1.3382344 (acccessed 2024/03/03/05:56:38). From DOI.org (Crossref).

(6) Grimme, S.; Ehrlich, S.; Goerigk, L. Effect of the damping function in dispersion corrected density functional theory. *Journal of Computational Chemistry* **2011**, *32* (7), 1456-1465. DOI: 10.1002/jcc.21759 (acccessed 2024/04/08/21:46:52). From DOI.org (Crossref).

(7) Blöchl, P. E. Projector augmented-wave method. *Physical Review B* **1994**, *50* (24), 17953-17979. DOI: 10.1103/PhysRevB.50.17953 (acccessed 2024/04/09/03:25:35). From DOI.org (Crossref).

(8) Kresse, G.; Joubert, D. From ultrasoft pseudopotentials to the projector augmented-wave method. *Physical Review B* **1999**, *59* (3), 1758-1775. DOI: 10.1103/PhysRevB.59.1758 (acccessed 2024/04/09/03:25:05). From DOI.org (Crossref).

(9) Neese, F.; Wennmohs, F.; Becker, U.; Riplinger, C. The ORCA quantum chemistry program package. *The Journal of Chemical Physics* **2020**, *152* (22), 224108. DOI: 10.1063/5.0004608 (acccessed 2023/03/20/19:34:03). From DOI.org (Crossref).

(10) Zheng, J.; Xu, X.; Truhlar, D. G. Minimally augmented Karlsruhe basis sets. *Theoretical Chemistry Accounts* **2011**, *128* (3), 295-305. DOI: 10.1007/s00214-010-0846-z (acccessed 2023/10/02/15:17:37). From DOI.org (Crossref).

(11) Heyden, A.; Bell, A. T.; Keil, F. J. Efficient methods for finding transition states in chemical reactions: Comparison of improved dimer method and partitioned rational function optimization method. *The Journal of Chemical Physics* **2005**, *123* (22), 224101. DOI: 10.1063/1.2104507 (acccessed 2024/03/30/22:44:17). From DOI.org (Crossref).

(12) Qi, J.; Finzel, J.; Robatjazi, H.; Xu, M.; Hoffman, A. S.; Bare, S. R.; Pan, X.; Christopher, P. Selective Methanol Carbonylation to Acetic Acid on Heterogeneous Atomically Dispersed ReO4/SiO2 Catalysts. *Journal of the American Chemical Society* **2020**, *142* (33), 14178-14189. DOI: 10.1021/jacs.0c05026 (acccessed 2022/03/02/19:28:25). From ACS Publications.

(13) Boronat, M.; Martínez-Sánchez, C.; Law, D.; Corma, A. Enzyme-like Specificity in Zeolites: A Unique Site Position in Mordenite for Selective Carbonylation of Methanol and Dimethyl Ether with CO. *Journal of the American Chemical Society* **2008**, *130* (48), 16316-16323. DOI: 10.1021/ja805607m (acccessed 2022/05/19/20:55:36). From DOI.org (Crossref).

(14) Cai, K.; Li, Y.; Shen, H.; Cheng, Z.; Huang, S.; Wang, Y.; Ma, X. A density functional theory study on the mechanism of Dimethyl ether carbonylation over heteropolyacids catalyst. *Frontiers of Chemical Science and Engineering* **2021**, *15* (2), 319-329. DOI: 10.1007/s11705-020-1957-2 (acccessed 2024/03/30/23:40:44). From DOI.org (Crossref).

(15) Goodrow, A.; Bell, A. T.; Head-Gordon, M. Are Spin-Forbidden Crossings a Bottleneck in Methanol Oxidation? *The Journal of Physical Chemistry C* **2009**, *113* (45), 19361-19364. DOI: 10.1021/jp906603r.

(16) Sundstrom, E. J.; Yang, X.; Thoi, V. S.; Karunadasa, H. I.; Chang, C. J.; Long, J. R.; Head-Gordon, M. Computational and experimental study of the mechanism of hydrogen generation from water by a

molecular molybdenum-oxo electrocatalyst. *J Am Chem Soc* **2012**, *134* (11), 5233-5242. DOI: 10.1021/ja210949r From NLM Medline.